Journal of Sound and Vibration (2001) **245**(4), 633–652
doi:10.1006/jsvi.2000.3556, available online at http://www.idealibrary.com on IDEAL®

A 3-D HIERARCHICAL FE FORMULATION OF BIOT'S EQUATIONS FOR ELASTO-ACOUSTIC MODELLING OF POROUS MEDIA

N.-E. Hörlin, M. Nordström and P. Göransson

Department of Vehicle Engineering, Royal Institute of Technology, 100 44 *Stockholm, Sweden*

(*Received* 4 *February* 2000, *and in final form* 11 *December* 2000)

A three-dimensional hierarchical finite element formulation of Biot's equation for low frequency elasto-acoustic wave propagation in fluid saturated porous media based on a weak formulation with fluid displacement and solid displacement as dependent variables is presented. A global error measure for evaluation of the convergence is proposed. Numerical simulations of an air saturated polyurethane foam material show faster convergence for the hierarchical extensions than for linear and quadratic serendipity finite element mesh refinement extensions.

1. INTRODUCTION

Flexible lightweight fluid-saturated porous materials are commonly used in aircraft and ground transportation vehicles for a thermal insulation and as a sound absorbing material. Since virtual design has become very important in the automotive industry, the interest of numerical noise and vibration simulation tools for porous materials has increased. An accurate modelling of such materials at an early design stage is crucial to obtain optimal noise and vibration performance. To model mechanical waves being transmitted through and dissipated in the porous material for noise control purposes, the elastic and dissipative properties of both the solid frame and the saturating fluid has to be taken into account. Exceptions may be made for some cases where idealized simplifications are adequate e.g. rigid frame and infinitely flexible frame.

Biot presented in 1956 [1] a three-dimensional theory for coupled frame-fluid wave propagation in fluid saturated porous media, treating the solid frame and the saturating fluid as two separate co-located coupled continua. Two second order coupled complex partial differential equations were derived from this theory.

Three-dimensional finite element solutions to Biot's equations for elasto-acoustic wave propagation, have been extensively discussed in the literature during the last decade: see e.g., references [2–5]. Differing in the choice of dependent variables, i.e., frame displacement in conjunction with either fluid displacement; fluid pressure; fluid displacement and fluid pressure; fluid displacement potential and fluid pressure, most work published till date has invoked the use of a traditional FE basis; i.e., linear and quadratic shape functions.

A common concern of all the different FE solutions of Biot's equations is the question of convergence. It is clear that an FE basis good enough to yield a required accuracy in the predicted results, may be constructed through a refinement of the mesh (h-convergence). However, as an alternative to mesh refinement the FE basis may be enriched with

0022-460X/01/340633 + 20 $35.00/0

polynomials with increasingly higher degree until the required accuracy is obtained (p-convergence).

With the aim of finding more efficient numerical solution methods of Biot's equation, the contribution of this paper is to apply a *hierarchical finite element basis* on a Bubnov–Galerkin formulation of the Biot equations using the solid displacement and the fluid displacement as dependent variables. This choice of dependent variables gives a symmetric formulation and hence a symmetric system of equations without any assumptions of rotational free fluid. The symmetry of the equations has benefits while many commercial FE codes use symmetric equation solvers. On the contrary, the fluid pressure formulation gives an unsymmetric formulation and the fluid displacement potential, fluid pressure formulation gives a symmetric formulation but imposes rotational free assumption on the fluid.

The hierarchical basis used is a generalization of a two-dimensional hierarchical basis, introduced by Houmat 1997 [6], into three dimensions. An augmented Hooke's law (AHL) damping description of the solid frame based on augmented thermodynamic fields presented by Dovstam 1995 [7] and 1997 [8] (see Appendix B) is included in the formulation.

A three-dimensional numerical example involving material data of an air saturated polyurethane foam, is presented. The convergence of hierarchical extensions (*p*-extensions) of a single element is studied in terms of a proposed global error measure suitable for complex partial differential equations of this kind.

Since this paper focuses on the hierarchical formulation and the convergence, issues concerning the complexity of the implementation of hierarchical FEM, e.g., coupling between elements, Gauss quadratures and derivatives for curve-linear geometries will be left out to be discussed in a forthcoming paper. The convergence of the *p*-extensions is compared with mesh refinement extensions (*h*-extensions) of hexahedronal linear 8-node element and 20-node quadratic serendipity elements [9] for the purpose of investigating the computational efficiency of the p-method in this application.

2. VARIATIONAL FORMULATION OF THE 3-D BIOT EQUATIONS

Upon assuming a time harmonic variation, Biot's equations may be written in Cartesian tensor components as

$$(\hat{\mu} u^s_{i,j})_{,j} + ((\hat{\lambda} + \hat{\mu}) u^s_{j,j})_{,i} + (\omega^2 \rho_{11} - \mathrm{i}\omega b) u^s_i + (Q u^f_{j,j})_{,i} + (\omega^2 \rho_{12} + \mathrm{i}\omega b) u^f_i = 0, \quad (1a)$$

$$(Q u^s_{j,j})_{,i} + (\omega^2 \rho_{12} + \mathrm{i}\omega b) u^s_i + (R u^f_{j,j})_{,i} + (\omega^2 \rho_{22} - \mathrm{i}\omega b) u^f_i = 0. \quad (1b)$$

All material parameters are defined in Appendices G and B.

Assume constant material properties in a regular domain $\Omega \in R^3$ bounded by $\Gamma \in R^3$. Equations (1a) and (1b) are first multiplied with arbitrary, piecewise differentiable, linearly independent, real-valued weight functions v^s_i and v^f_i and are then integrated over the domain Ω to obtain a weak form of Biot's equations. The weight functions are restricted to satisfying homogenous Dirichlet boundary conditions on those parts of the boundary where Dirichlet conditions (not necessarily homogeneous) are imposed. The integrals are expressed here in the form of *inner products* which are defined in Appendix A:

$$(\hat{\mu} u^s_{i,jj} + (\hat{\lambda} + \hat{\mu}) u^s_{j,ji} + (\omega^2 \rho_{11} - \mathrm{i}\omega b) u^s_i, v^s_i)_\Omega + (Q u^f_{j,ji} + (\omega^2 \rho_{12} + \mathrm{i}\omega b) u^f_i, v^s_i)_\Omega = 0, \quad (2a)$$

$$(Q u^s_{j,ji} + (\omega^2 \rho_{12} + \mathrm{i}\omega b) u^s_i, v^f_i)_\Omega + (R u^f_{j,ji} + (\omega^2 \rho_{22} - \mathrm{i}\omega b) u^f_i, v^f_i)_\Omega = 0. \quad (2b)$$

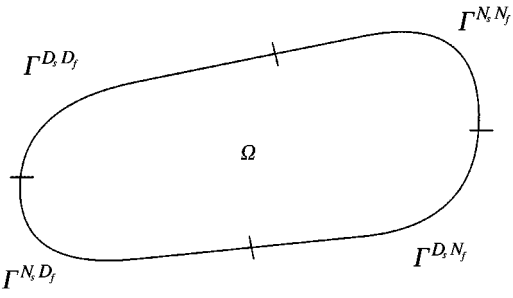

Figure 1. Schematic sketch of the domain with boundary conditions. (D means Dirichlet and N means Neumann boundary conditions.)

Integration by parts of equations (2a) and (2b) yields

$$\hat{\mu}(u^s_{i,j}, v^s_{i,j})_\Omega + \hat{\mu}(u^s_{j,i}, v^s_{i,j})_\Omega + \hat{\lambda}(u^s_{j,j}, v^s_{i,i})_\Omega - \omega^2\rho_{11}(u^s_i, v^s_i)_\Omega + \mathrm{i}\omega b(u^s_i, v^s_i)_\Omega$$

$$+ Q(u^f_{j,j}, v^s_{i,i})_\Omega - \omega^2\rho_{12}(u^f_i, v^s_i)_\Omega - \mathrm{i}\omega b(u^f_i, v^s_i)_\Omega = (\hat{T}_i, v^s_i)_{\Gamma_s} + \frac{Q}{R}(-p^f n_i, v^s_i)_{\Gamma_s} \tag{3a}$$

$$Q(u^s_{j,j}, v^f_{i,i})_\Omega - \omega^2\rho_{12}(u^s_i, v^f_i)_\Omega - \mathrm{i}\omega b(u^s_i, v^f_i)_\Omega + R(u^f_{j,j}, v^f_{i,i})_\Omega - \omega^2\rho_{22}(u^f_i, v^f_i)_\Omega$$

$$+ \mathrm{i}\omega b(u^f_i, v^f_i)_\Omega = \frac{Q}{3\hat{K}}(-p^s n_i, v^f_i)_{\Gamma_f} + (-p^f n_i, v^f_i)_{\Gamma_f}. \tag{3b}$$

The boundary Γ is divided into four parts, see Figure 1, and the boundary conditions are formulated as

$$u^s_i = 0, \quad u^f_i = 0 \text{ on } \Gamma^{D_s D_f}, \tag{4a}$$

$$\hat{\mu}(u^s_{i,j} + u^s_{j,i}) + \hat{\lambda}u^s_{k,k}\delta_{ij} = \hat{\sigma}_{ij}, \quad u^f_i = 0 \text{ on } \Gamma^{N_s D_f}, \tag{4b}$$

$$u^s_i = 0, \quad -Ru^f_{j,j} = p^f \text{ on } \Gamma^{D_s N_f}, \tag{4c}$$

$$\hat{\mu}(u^s_{i,j} + u^s_{j,i}) + \hat{\lambda}u^s_{k,k}\delta_{ij} = \hat{\sigma}_{ij}, \quad -Ru^f_{j,j} = p^f \text{ on } \Gamma^{N_s N_f} \tag{4d}$$

and $\Gamma_s \stackrel{\text{def}}{=} \Gamma^{N_s D_f} + \Gamma^{N_s N_f}$, $\Gamma_f \stackrel{\text{def}}{=} \Gamma^{D_s N_f} + \Gamma^{N_s N_f}$, $\hat{T}_i = \hat{\sigma}_{ij}n_j$ is the traction vector on Γ_s, n_i is the unit normal vector to the boundary Γ, $\hat{\sigma}_{ij} = \hat{\mu}(u^s_{i,j} + u^s_{j,i}) + \hat{\lambda}u^s_{k,k}\delta_{ij}$ is the AHL stress tensor for the homogenized solid frame on Γ_s, $p^f = -Ru^f_{j,j}$ is the homogenized fluid phase pressure on Γ_f and is related to the homogenized pressure in the pores by $p^f = \phi p^{pore}$, $\hat{p}^s = -\hat{\sigma}_{jj} = -3\hat{K}u^s_{j,j}$ is the AHL homogenized pressure in the solid frame on Γ_s and the AHL bulk modulus of the solid phase $\hat{K} = \hat{\lambda} + \frac{2}{3}\hat{\mu}$.

3. DERIVATION OF THE DYNAMIC STIFFNESS MATRIX AND LOAD VECTOR

Define discrete approximations to $u_i^s(\mathbf{x})$ and $u_i^f(\mathbf{x})$ as finite sums of trial functions multiplied by undetermined coefficients:

$$u_{Ni}^s(\mathbf{x}) \stackrel{\text{def}}{=} \sum_{m=1}^{N_i^s} c_{im}^s \varphi_i^m(\mathbf{x}), \quad u_{Ni}^f(\mathbf{x}) \stackrel{\text{def}}{=} \sum_{q=1}^{N_i^f} c_{iq}^f \psi_i^q(\mathbf{x}). \tag{5}$$

Essentially the same basis is used for the test functions as for the trial functions except that those functions not fulfilling the restrictions described in previous section are excluded:

$$v_j^s = \varphi_j^m(\mathbf{x}), \quad v_j^f = \psi_j^q(\mathbf{x}). \tag{6}$$

If equations (5) and (6) are inserted in equations (3a) and (3b) the boundary value problem turns into a finite set of simultaneous linear equations of the form

$$\begin{bmatrix} \mathbf{K}^s & \mathbf{K}^{sf} \\ \mathbf{K}^{fs} & \mathbf{K}^f \end{bmatrix} \begin{bmatrix} \mathbf{c}^s \\ \mathbf{c}^f \end{bmatrix} = \begin{bmatrix} \mathbf{f}^s \\ \mathbf{f}^f \end{bmatrix}, \tag{7}$$

where $\mathbf{c}^s \stackrel{\text{def}}{=} \{c_{im}^s\}$, $\mathbf{c}^f \stackrel{\text{def}}{=} \{c_{iq}^f\}$, and $\mathbf{f}^s \stackrel{\text{def}}{=} \{ f_j^{(s)^n}\}$, $\mathbf{f}^f \stackrel{\text{def}}{=} \{ f_j^{(f)^r}\}$.

The elements of the submatrices of the dynamic stiffness matrix and the right-hand side are derived as

$$K_{ji}^{(s)^{nm}} = \sum_{k=1}^{3} \hat{\mu}(\varphi_{i,k}^m, \varphi_{j,k}^n)_\Omega \delta_{ij} + \hat{\mu}(\varphi_{i,j}^m, \varphi_{j,i}^n)_\Omega + \hat{\lambda}(\varphi_{i,i}^m, \varphi_{j,j}^n)_\Omega$$

$$- \omega^2 \rho_{11}(\varphi_i^m, \varphi_j^n)_\Omega + \mathrm{i}\omega b(\varphi_i^m, \varphi_j^n)_\Omega, \tag{8a}$$

$$K_{ji}^{(sf)^{nq}} = Q(\psi_{i,i}^q, \varphi_{j,j}^n)_\Omega - \omega^2 \rho_{12}(\psi_i^q, \varphi_j^n)_\Omega - \mathrm{i}\omega b(\psi_i^q, \varphi_j^n)_\Omega, \tag{8b}$$

$$K_{ji}^{(fs)^{rm}} = Q(\varphi_{i,i}^m, \psi_{j,j}^r)_\Omega - \omega^2 \rho_{12}(\varphi_i^m, \psi_j^r)_\Omega - \mathrm{i}\omega b(\varphi_i^m, \psi_j^r)_\Omega, \tag{8c}$$

$$K_{ji}^{(f)^{rq}} = R(\psi_{i,i}^q, \psi_{j,j}^r)_\Omega - \omega^2 \rho_{22}(\psi_i^q, \psi_j^r)_\Omega + \mathrm{i}\omega b(\psi_i^q, \psi_j^r)_\Omega, \tag{8d}$$

$$f_j^{(s)^n} = (\hat{T}_j, \varphi_j^n)_{\Gamma_s} + (Q/R)(-p^f n_j, \varphi_j^n)_{\Gamma_s}, \tag{9a}$$

$$f_j^{(f)^r} = (Q/3K)(-\hat{p}^s n_j, \psi_j^r)_{\Gamma_f} + (-p^f n_j, \psi_j^r)_{\Gamma_f}, \tag{9b}$$

$$i \in \{1, 2, 3\}, \quad j \in \{1, 2, 3\}, \tag{10}$$

$$m \in \{1, 2, \ldots, N_i^s\}, \quad n \in \{1, 2, \ldots, N_j^s\},$$

$$r \in \{1, 2, \ldots, N_i^f\}, \quad q \in \{1, 2, \ldots, N_j^f\} \tag{11}$$

(no summation convention over i and j in equations (8a)–(9b)).

Due to the choice of test functions, $\mathbf{K}^{sf} = \mathbf{K}^{fs^{\mathrm{T}}}$ if no inhomogenous Dirichlet conditions are imposed. Otherwise some elements of $\mathbf{c}^s$ and/or $\mathbf{c}^f$ are prescribed to approximate the displacement on those parts of the boundary where the Dirichlet conditions are imposed. The equation system will then be reduced to a symmetric system where the prescribed d.o.f.

(degrees of freedom) are removed from the unknown in the left-hand side and are moved to the right-hand side.

4. HIERARCHICAL FINITE ELEMENT BASIS

The previous section dealt with an arbitrary regular domain. In this section, a single, parallelepiped-shaped finite element subdomain will be considered. Coupling conditions between hierarchical elements (compatibility and equilibrium) will not be discussed in the present paper. The hierarchical basis is defined by the function terms in function series (5). The m_ith term of the ith component direction is given by the product of three polynomial functions as follows:

$$\varphi_i^{m_i}(\mathbf{x}) \stackrel{\text{def}}{=} \prod_{k=1}^{3} f_{l_k}\left(\frac{2x_k}{L_k}\right), \quad \frac{2x_k}{L_k} \in [-1, 1], \tag{12}$$

where

$$k \in \{1, 2, 3\} \tag{13}$$

is the ordinal number of the spatial co-ordinate direction,

$$i \in \{1, 2, 3\} \tag{14}$$

the ordinal number of the displacement component direction

$$l_k \in \{1, \ldots, p_k^i + 2\}, \tag{15}$$

the polynomial number for the kth co-ordinate direction, and p_k^i is the number of hierarchical polynomials for the ith displacement component in the kth spatial co-ordinate direction. Finally,

$$m_i = [(l_1 - 1)(p_2^i + 2) + l_2 - 1](p_3^i + 2) + l_3 \tag{16}$$

is the ordinal number of the term in the ith direction. From equations (15) and (16) it is clear that

$$N_i^s = \prod_{k=1}^{3} (p_k^i + 2). \tag{17}$$

Upon omitting the co-ordinate direction subscript k, the polynomials f_l in equation (12) are defined as

$$f_l(\chi) \stackrel{\text{def}}{=} \begin{cases} \dfrac{1}{2}(1 - \chi), & l = 1, \\ \dfrac{1}{2}(1 + \chi), & l = 2, \\ \displaystyle\sum_{s=0}^{\text{int}(l/2)} \frac{(-1)^s (2l - 2s - 5)!!}{2^s s!(l - 2s - 1)!} \chi^{l-2s-1}, & l \geqslant 3. \end{cases} \tag{18}$$

$\psi_i^q(\mathbf{x})$ is defined in a similar way as $\varphi_i^m(\mathbf{x})$.

It may be noted that for $p = 0$ and 1 the coefficients c_{im}^s and c_{iq}^f in equation (5) are interpreted as *nodal* displacements for ordinary linear and quadratic Lagrange elements respectively. For $p > 1$ such interpretations cannot be made.

The functions f_l, $l > 2$, are called *hierarchical functions* and p is subsequently the number of these. Hence the highest occurring polynomial degree is $p + 1$. These functions are derived from Rodrigue's form of the Legendre orthogonal polynomials [6]. The first eight hierarchical functions are shown in Appendix C.

5. CONVERGENCE

In this section, a global error measure which is easy to compute is proposed. The theory is not limited to the hierarchical basis but can be applied on any FE basis feasible for this kind of problems.

Define $\mathbf{u}^s \overset{\text{def}}{=} \{u_i^s\}$, $\mathbf{u}^f \overset{\text{def}}{=} \{u_i^f\}$. Equations (1a) and (1b) may be written in the form

$$\begin{bmatrix} \mathbf{L}^{ss} & \mathbf{L}^{sf} \\ \mathbf{L}^{fs} & \mathbf{L}^{ff} \end{bmatrix} \begin{bmatrix} \mathbf{u}^s \\ \mathbf{u}^f \end{bmatrix} = \mathbf{0}, \tag{19}$$

where $\mathbf{L}^{ss}$, $\mathbf{L}^{sf}$, $\mathbf{L}^{fs}$ and $\mathbf{L}^{ff}$ are the linear differential operators in equations (1a) and (1b). Further, define $\mathbf{v}^s \overset{\text{def}}{=} \{v_i^s\}$, $\mathbf{v}^s \overset{\text{def}}{=} \{v_i^s\}$. Due to the linear independence between $\mathbf{v}^s$ and $\mathbf{v}^f$, equations (2a) and (2b) may be written as one scalar equation:

$$\left(\begin{bmatrix} \mathbf{L}^{ss} & \mathbf{L}^{sf} \\ \mathbf{L}^{fs} & \mathbf{L}^{ff} \end{bmatrix} \begin{bmatrix} \mathbf{u}^s \\ \mathbf{u}^f \end{bmatrix}, \begin{bmatrix} \mathbf{v}^s \\ \mathbf{v}^f \end{bmatrix} \right)_\Omega = 0. \tag{20}$$

Equation (20) suggests that the solid and fluid displacement can be treated as one six-dimensional displacement field instead of two three-dimensional ones. This enables the use of a more compact formalism in this section. Introduce the six-dimensional displacement vectors

$$\mathbf{u} \overset{\text{def}}{=} \begin{bmatrix} \mathbf{u}^s \\ \mathbf{u}^f \end{bmatrix}, \quad \mathbf{v} \overset{\text{def}}{=} \begin{bmatrix} \mathbf{v}^s \\ \mathbf{v}^f \end{bmatrix}. \tag{21}$$

Define a sesquilinear form $B(\mathbf{u}, \mathbf{v})$ as the sum of the left-hand sides of equations (3a), (3b) and the antilinear form $F(\mathbf{v})$ as the sum of the boundary terms: i.e., the right-hand sides of equations (3a), (3b) (see Appendix D). These right-hand sides represent all external loads imposed and are called the external virtual work. (This is equivalent to integrating equation (20) by parts and collecting the boundary terms on the right-hand side and the volume terms on the left-hand side.)

Then the weak boundary value problem in equations (3a) and (3b) may be written in the compact form:

$$\begin{cases} \text{Find } \mathbf{u} \in V = \{\mathbf{v} | \mathbf{v} \in \mathscr{H}^1(\Omega), & \mathbf{v}^s = \mathbf{v}_\Gamma^s \text{ on } (\Gamma^{D_s D_f} + \Gamma^{D_s N_f}), \\ & \mathbf{v}^f = \mathbf{v}_\Gamma^f \text{ on } (\Gamma^{D_s D_f} + \Gamma^{N_s D_f})\}, \\ B(\mathbf{u}, \mathbf{v}) = F(\mathbf{v}) \ \forall \mathbf{v} \in V^0 = \{\mathbf{v} | \mathbf{v} \in \mathscr{H}^1(\Omega), & \mathbf{v}^s = \mathbf{0} \text{ on } (\Gamma^{D_s D_f} + \Gamma^{D_s N_f}), \\ & \mathbf{v}^f = \mathbf{0} \text{ on } (\Gamma^{D_s D_f} + \Gamma^{N_s D_f})\}, \end{cases} \tag{22}$$

where

$$\mathscr{H}^1(\Omega) \stackrel{\text{def}}{=} H^1(\Omega) \times H^1(\Omega) \times H^1(\Omega) \times H^1(\Omega) \times H^1(\Omega) \times H^1(\Omega) \tag{23}$$

is the Cartesian product between six Sobolev spaces, one for each displacement component. The corresponding finite-dimensional problem

$$\left\{ \begin{array}{l} \text{Find } \mathbf{u}_{FE} \in V_{FE} \subset V \\ B(\mathbf{u}_{FE}, \mathbf{v}) = F(\mathbf{v}) \ \forall \mathbf{v} \in V^0_{FE} \subset V^0 \end{array} \right\} \tag{24}$$

on the finite dimensional finite element subspace V_{FE} has a unique solution which is an approximate solution to equation (22) and is called the B-orthogonal projection onto V_{FE} of the exact solution in the sense of

$$B(\mathbf{u}, \mathbf{v}) = B(\mathbf{u}_{FE}, \mathbf{v}) \ \forall \mathbf{v} \in V^0_{FE}, \tag{25}$$

according to equations (22) and (24).

Now, the error function is defined as

$$\mathbf{e} \stackrel{\text{def}}{=} \mathbf{u} - \mathbf{u}_{FE}, \tag{26}$$

and a global measure of the error is defined as

$$\mathscr{E} = |F(\bar{\mathbf{e}})|^{\frac{1}{2}}. \tag{27}$$

The proposed measure may be proven to be *bounded* by the square root of the $\mathscr{H}^1(\Omega)$-norm of the error (see Appendix E). Thus it follows that $\mathscr{E}$ goes to zero as the approximate solution converges in the $\mathscr{H}^1(\Omega)$-norm. However, the error measure is not proven to be *bounded below* by the same norm.

In the present paper, no mathematical theory for an *a priori* or a *posteriori* error estimate based on this error measure will be developed. The global error measure $\mathscr{E}$ is used here to study the convergence of hierarchical extensions compared to mesh refinement extensions. A problem that occurs is that the exact solution which has to be known to calculate the error function is not available. However, an approximate solution with an error, orders of magnitude smaller than that of the studied extensions, may be used as reference instead of the exact solution. Such approximate solutions are referred to here as *reference solutions.*

In order to compare the quality of solutions for different frequencies or with different loads, a *relative error measure* is defined as the one in equation (27) but normalized with $|F(\bar{\mathbf{u}})|^{\frac{1}{2}}$: i.e.,

$$\mathscr{E}_{rel} \stackrel{\text{def}}{=} \frac{|F(\bar{\mathbf{e}})|^{\frac{1}{2}}}{|F(\bar{\mathbf{u}})|^{\frac{1}{2}}}, \tag{28}$$

which may also be written as

$$\mathscr{E}_{rel} = \left| \frac{F(\bar{\mathbf{u}}) - F(\bar{\mathbf{u}}_{FE})}{F(\bar{\mathbf{u}})} \right|^{\frac{1}{2}}. \tag{29}$$

If a reference solution is used instead of the exact solution the error measure is approximated to

$$\mathscr{E}_{rel} \approx \left| \frac{F(\bar{\mathbf{u}}_{ref}) - F(\bar{\mathbf{u}}_{FE})}{F(\bar{\mathbf{u}}_{ref})} \right|^{\frac{1}{2}}. \tag{30}$$

This approximation will be used to evaluate the convergence in the next section. $F(\bar{\mathbf{u}}_{FE})$ is easily computed from the vector scalar product of the result displacement vector and the load vector in the FE matrix equation (7): i.e.,

$$F(\bar{\mathbf{u}}_{FE}) = \begin{bmatrix} \mathbf{c}^s \\ \mathbf{c}^f \end{bmatrix}^t \begin{bmatrix} \mathbf{f}^s \\ \mathbf{f}^f \end{bmatrix}. \tag{31}$$

6. NUMERICAL EXAMPLE

As a numerical example a parallelepiped-shaped domain with dimensions $L_1 = 0{\cdot}2\,\text{m}$, $L_2 = 0{\cdot}3\,\text{m}$, $L_3 = 0{\cdot}5\,\text{m}$ and material parameters representing a polyurethane foam material with open cell structure is used. The material data are given in Appendix F. Features of this material are discussed in reference [14].

Both the solid frame and the fluid are considered free (i.e., homogenous Neumann condition) on all boundaries except on the boundary surface at $x_3 = -L_3/2$, where a uniformly distributed load is applied exclusively on the solid frame in the positive 3 direction (i.e. $\text{Re}[\hat{T}_3] > 0$, $\text{Im}[\hat{T}_3] = \hat{T}_1 = \hat{T}_2 = 0$). Note that this load is exactly represented in the hierarchical basis for $p = 0$ and hence for any p and also for any basis of mesh refinement extensions.

The displacements were calculated for 30 equally distant frequencies in the interval 10–300 Hz. In the calculations performed, the values of p were set to be equal for all displacement components in all co-ordinate directions, although this is not necessary in the proposed formulation which allows the values to be different, possibly allowing higher computational efficiency to be reached.

7. RESULT AND DISCUSSION

In the present study, the result of $p = 16$ has been used as a *reference solution* for frequencies up to 190 Hz. If the FE approximation converges to the exact solution with increasing p, the difference between $F(\bar{\mathbf{u}}_{FE})$ of two consecutive extensions converges to zero. Figure 2 strongly indicates that the error for $p = 16$ may be neglected in comparison with the error for $p = 11$ and that the result for $p = 16$ can be used as a reference instead of the exact solution when estimating the error for $p \leqslant 11$. One may observe that when the $p = 11$ solution is very accurate at low frequencies the quotient is quite small, but at higher frequencies when the $p = 11$ solution becomes less accurate the quotient is large as the $p = 16$ solution is still very accurate, and at even higher frequencies when the $p = 16$ solution also becomes less accurate, the quotient is again small. Thus, the $p = 16$ solution is much more accurate than the $p = 11$ solution in the actual frequency range 10–300 Hz and the $p = 16$ solution is consequently an accurate reference solution when studying the convergence rate of hierarchical extension at least up to $p = 11$.

The convergence in $\mathscr{E}_{rel}$ for a sample of frequencies 30–290 Hz is shown in Figure 3. A type of "cut-on" phenomenon, i.e., the speed of convergence rapidly increase at different

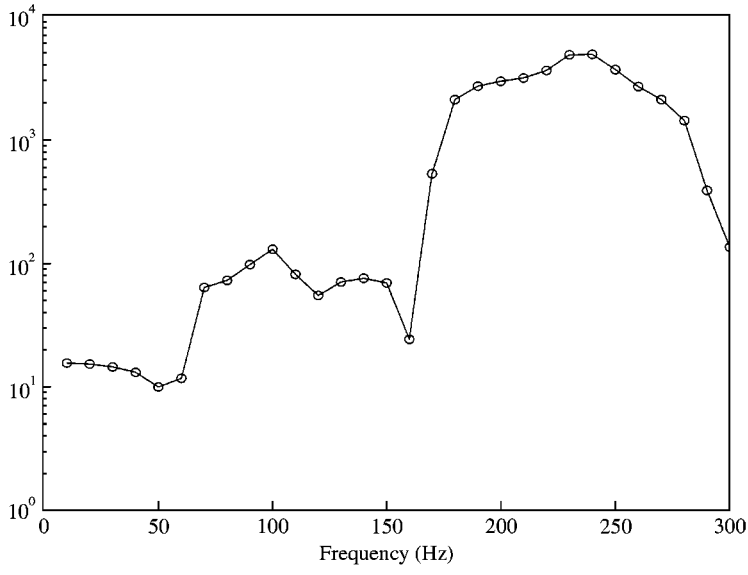

Figure 2. $\dfrac{F(\bar{\mathbf{u}}_{FE})^{(p=12)} - F(\bar{\mathbf{u}}_{FE})^{(p=11)}}{F(\bar{\mathbf{u}}_{FE})^{(p=16)} - F(\bar{\mathbf{u}}_{FE})^{(p=15)}}$ versus frequency (Hz).

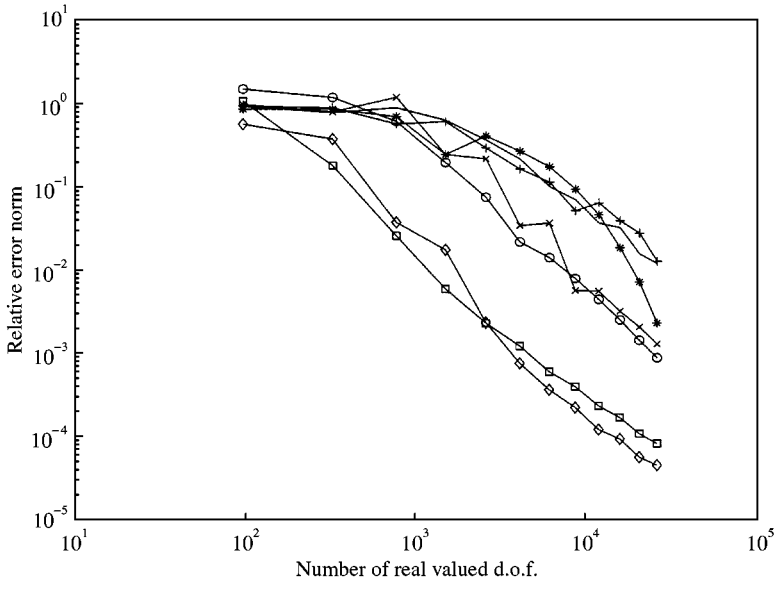

Figure 3. Convergence in $\mathscr{E}_{rel}$ for hierarchical extension $p = 0$ to 11 at different frequencies 30–290 Hz. –□–, 30 Hz; –◇–, 50 Hz; –○–, 90 Hz; –×–, 130 Hz; –*–, 170 Hz; —+–, 250 Hz; ——, 290 Hz.

polynomial degrees, is observed in the convergence at different polynomial degrees with different convergence rates for each frequency. The general trend is that for higher frequencies (and shorter wavelength) a higher polynomial degree is required for the convergence to cut on. However monotonic convergence is not guaranteed as seen in Figure 3, e.g., for 130 Hz, 250 Hz. *Monotonic* convergence is only guaranteed asymptotically

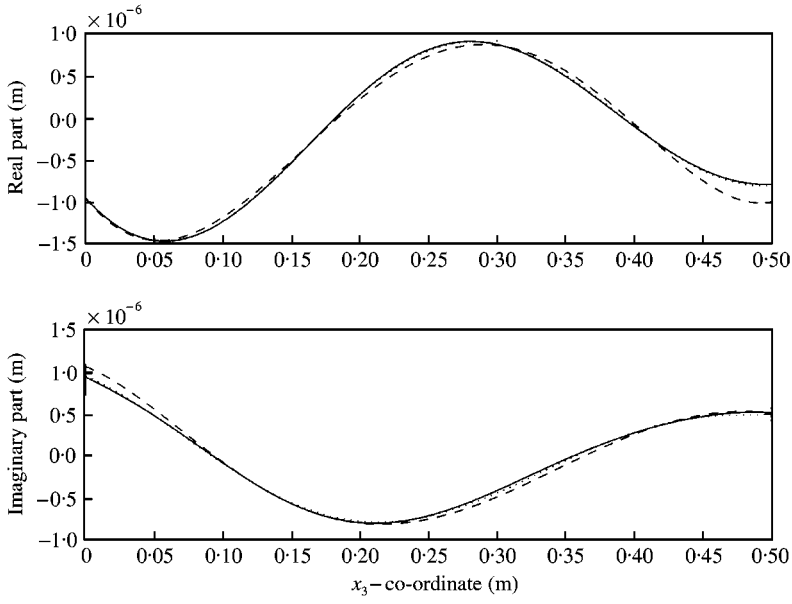

Figure 4. Solid phase displacement in 3 direction at 130 Hz for $x_1 = 0{\cdot}13$, $x_2 = 0{\cdot}21$, $0 \leqslant x_3 \leqslant 0{\cdot}5$ (real part). – – –, $p = 4$; ....., $p = 5$; ·–·–·, $p = 7$; ——, $p = 16$.

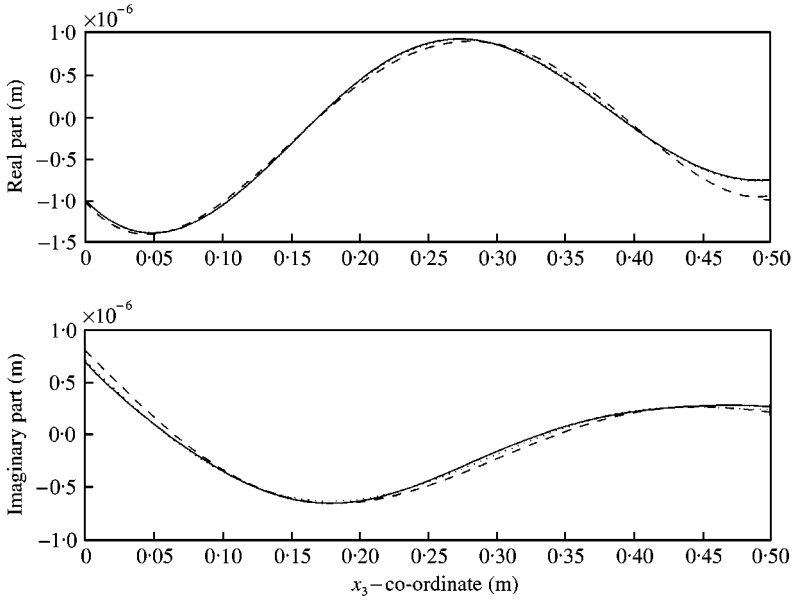

Figure 5. Fluid phase displacement in 3 direction at 130 Hz for $x_1 = 0{\cdot}13$, $x_2 = 0{\cdot}21$, $0 \leqslant x_3 \leqslant 0{\cdot}5$ (real part). – – –, $p = 4$; ....., $p = 5$; ·–·–·, $p = 7$; ——, $p = 16$.

when the number of d.o.f. approaches infinity [13]. The stair-like behavior which can be seen for some frequencies in Figure 3 is mainly due to assymetric or symmetric properties of the exact solution. Note that every second p provides an additional subset of symmetric or assymetric shape functions respectively.

h-extensions, using linear and quadratic shape functions, has been computed and the convergence compared with the hierarchical extensions in Figures 6–9. Linear extensions

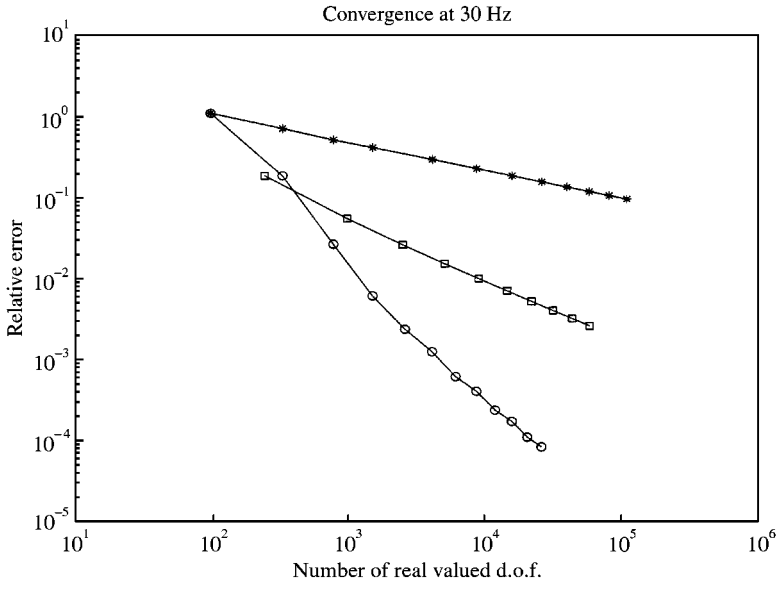

Figure 6. Convergence in $\mathscr{E}_{rel}$ for hierarchical extension $p = 0$ to 11 at 30 Hz compared with h-extensions of linear and quadratic elements. –*–, linear; –□–, quadratic; –○–, hierarchical.

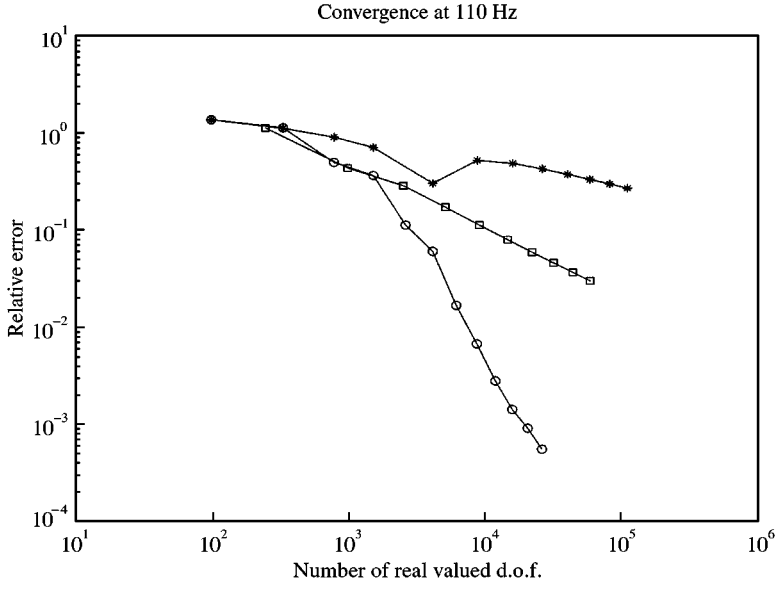

Figure 7. Convergence in $\mathscr{E}_{rel}$ for hierarchical extension $p = 0$ to 11 at 110 Hz compared with h-extensions of linear and quadratic elements. –*–, linear; –□–, quadratic; –○–, hierarchical.

were computed for 1, 2, 4, 8, 10, 12, 14, 16, 18, 20 elements and the quadratic serendipity extensions for 1–10 elements on each side of the parallelepiped-shaped domain. Note that $\mathscr{E}_{rel}$ for the hierarchical extension $p = 0$ always coincides with the linear h-extension for 1 element per side as expected because the solutions are identical. The same can be noticed for the serendipity extension for 1 element per side and the hierarchical extension for $p = 1$, but the coincidence is only approximative and the number of d.o.f. differ, because the

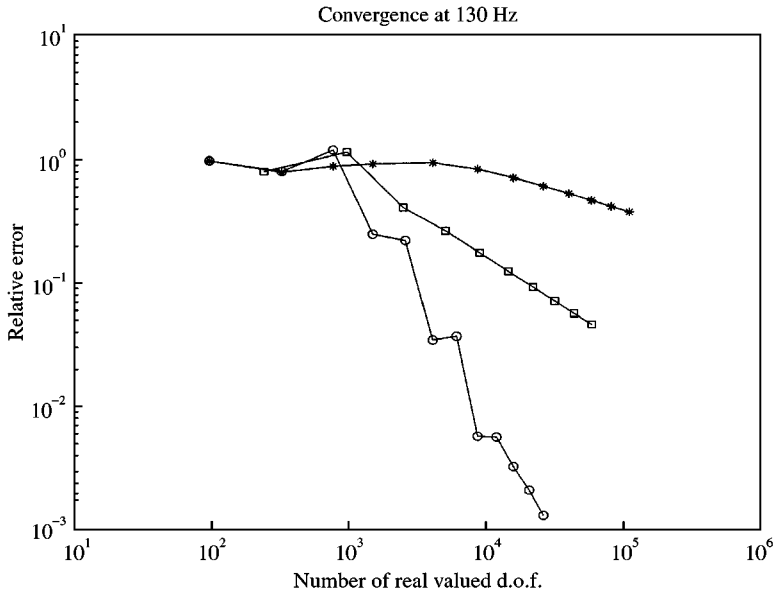

Figure 8. Convergence in $\mathscr{E}_{rel}$ for hierarchical extension $p = 0$ to 11 at 130 Hz compared with h-extensions of linear and quadratic elements. –*–, linear; –□–, quadratic; –○–, hierarchical.

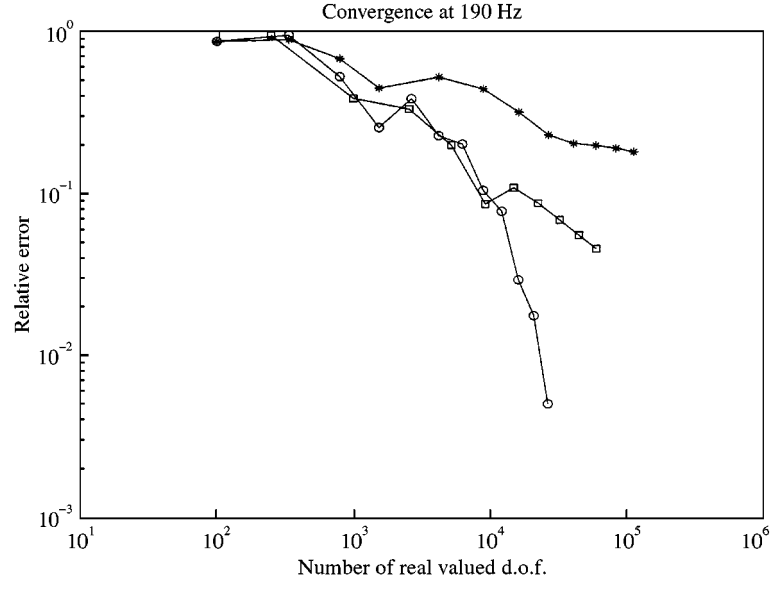

Figure 9. Convergence in $\mathscr{E}_{rel}$ for hierarchical extension $p = 0$ to 11 at 190 Hz compared with h-extensions of linear and quadratic elements. –*–, linear; –□–, quadratic; –○–, hierarchical.

serendipity element lacks the mid-surface and the mid-volume nodes. To illustrate what a certain value of $\mathscr{E}_{rel}$ corresponds to, the deformation of the solid phase of the porous material along a line inside the porous material has been included. A value of $\mathscr{E}_{rel}$ less than 10^{-2} corresponds to a solution which cannot be separated from the exact solution by visual inspection of a deformation plot, see e.g., for $p = 7$ at 130 Hz given in Figures 4, 5 and 8. It

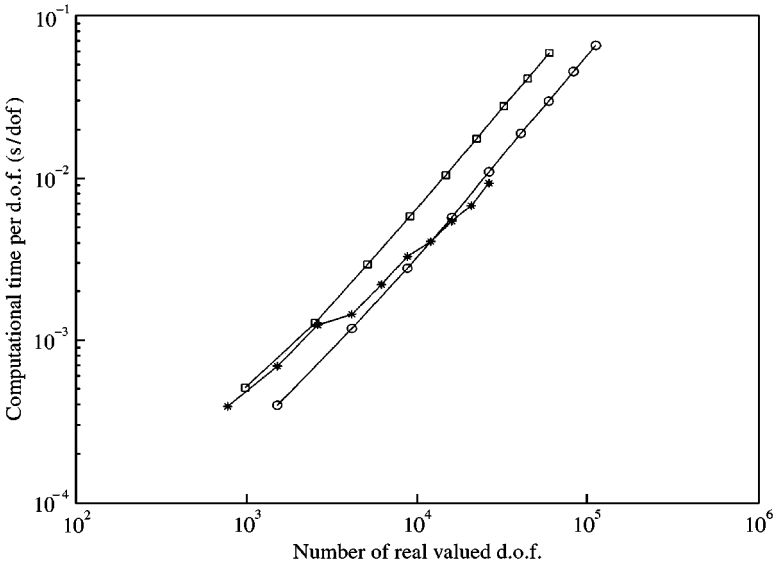

Figure 10. Computational time per degree of freedom for hierarchical extension $p = 0$ to 12 compared with h-extensions of linear and quadratic elements. –⊖–, linear; –⊞–, quadratic; –⁎–, hierarchical.

may also be noted that although the solid frame alone is excited by a distributed load, the fluid moves almost with the same amplitude as can be seen in Figures 4, 5.

As can be seen in Figure 10 the computational time per d.o.f. is of the same order of magnitude for the h-extensions and the p-extensions. A different symmetric solver was however used for the h-extensions than for the p-extensions.

For all calculated frequencies the hierarchical extensions converge considerably faster than the linear and the serendipity h-extensions when p exceeds a certain value, the convergence cut-on, which seems to increase with higher frequency. Below that value of p the hierarchical extensions converge at approximately the same rate as the serendipity h-extensions. In such a region some mesh refinements, keeping p constant, are possibly more efficient before increasing the value of p any further.

Figure 11 shows the absolute value of $\frac{1}{2}F(\bar{\mathbf{u}}_{FE})$ for $p = 10$ in the frequency interval 10–190 Hz. $\frac{1}{2}F(\bar{\mathbf{u}}_{FE})$ may, for real loads, be interpreted as

$$\left|\frac{1}{2}F(\bar{\mathbf{u}}_{FE})\right| = \left|\frac{P}{\omega}\right|, \tag{32}$$

where P is the complex power induced by the boundary load.

The peak at 62 Hz represents the fundamental eigenmode which has an antisymmetric one wavelength shape. Three to four other eigenmodes are identified in the frequency interval. No significantly different convergence behavior is observed close to resonance (e.g., at 60 Hz) than at other frequencies.

8. CONCLUSION

A hierarchical formulation of Biot's equations is presented and a numerical example shows faster convergence in terms of $\mathscr{E}_{rel}$ than h-extensions of linear and serendipic elements

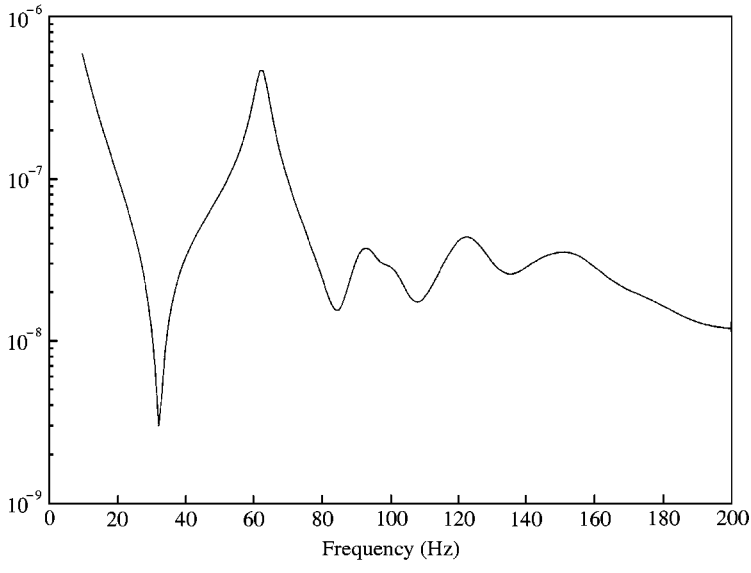

Figure 11. $|\frac{1}{2}F(\bar{\mathbf{u}}_{FE})|$ for $p = 10$ in the frequency interval 10–200 Hz.

especially when small errors are required. Further investigation of the *hp-convergence* (i.e., combined use of hierarchical extensions and mesh refinement) of this method is needed to choose an optimal strategy for finding a solution of required accuracy.

REFERENCES

1. M. A. BIOT 1956 *Journal of the Acoustic Society of America* **28**, 168–178. Theory of propagation of elastic waves in a fluid-saturated porous solid. Part I. Low-frequency range.
2. N. ATALLA, R. PANNETON and P. DEBERGUE 1998 *Journal of the Acoustic Society of America* **104**, Part 1. A mixed displacement–pressure formulation for porelastic materials.
3. V. EASWARAN, W. LAURIKS and J. P. COYETTE 1996 *Journal of the Acoustic Society of America* **100**. Displacement-based finite element method for guided wave propagation problems: Application to porelastic media.
4. M. DHAINAUT 1996 *Doctoral Thesis, Department of Telecommunications, Norwegian University of Science and Technology Trondheim*, Report 429612, Finite element procedures for fluid–structure interactions in acoustics.
5. P. GÖRANSSON 1998 *International Journal of Numerical Methods Engineering* **41**, 167–192. A 3-D symmetric, finite element formulation of the biot equations with application to acoustic wave propagation through an elastic porous medium.
6. A. HOUMAT 1997 *Journal of Sound and Vibration* **201**, 465–472. Hierarchical finite element analysis of the vibration of membranes.
7. K. DOVSTAM 1995 *International Journal of Solids and Structures* **32**, 2835–2852. Augmented Hooke's Law in frequency domain. A three dimensional material damping formulation.
8. K. DOVSTAM 1997 *International Journal of Solids and Structures* **34**, 2733–2754. Receptance model based on isotropic damping functions and elastic displacement modes.
9. O. C. ZIENKIEWICZ 1977 *The Finite Element Method*. New York: McGraw-Hill.
10. J. T. ODEN and L. F. DEMKOWICZ 1996 *Applied Functional Analysis*. Boca Rato, FL: CRC Press, Inc. ISBN 0-8493-2551-X.
11. B. A. SZABÓ and I. BABUŠKA 1991 *Finite Element Analysis*. New York: Wiley-Interscience, ISBN 0-471-50273-1.
12. T. LEKSZYCKI 1991 *Mechanics of Structures and Machines* **19**, 163–192. Application of Variational Methods in Analysis and Synthesis of Viscoelastic Continuous Systems.

13. F. IHLENBURG 1998 *Finite element analysis of acoustic scattering*. Berlin: Springer-Verlag, ISBN 0-387-98319-8.
14. P. GÖRANSSON 1998 *Doctoral Thesis, Department of Engineering Acoustics LTH Lund University Sweden*. Report TVBA-1006 ISSN: 0281-8477, Numerical modelling of dynamics of light porous materials.
15. B. DAYA REDDY 1997 *Introductory Functional Analysis: With Applications to Boundary Value Problems and Finite Elements*. Berlin: Springer-Verlag, ISBN 0-387-98307-4.

APPENDIX A: INNER PRODUCT NOTATION

The inner product operator is defined as

$$(\mathbf{V}, \mathbf{W})_{\Lambda} \stackrel{\text{def}}{=} \int_{\Lambda} \left(\sum_{i=1}^{M} V_i \bar{W}_i \right) \mathrm{d}\Lambda,$$

where $\mathbf{V}$ and $\mathbf{W}$ are vector functions with M elements each (or scalar functions when $M = 1$), Λ is the integration domain (line, surface or volume depending on the application). An overbar denotes complex conjugate.

APPENDIX B: AUGMENTED HOOKE'S LAW PARAMETERS

For isotropic material the augmented Hooke's law (AHL) Lamé moduli $\hat{\mu}$ and $\hat{\lambda}$ are defined as the corresponding static elastic parameters μ and λ which are related to the engineering elastic constants, Young's modulus E and the Poisson ratio v by

$$\mu = \frac{E}{2(1+v)}$$

and

$$\lambda = \frac{Ev}{(1+v)(1-2v)},$$

but augmented with complex frequency dependent damping functions $d_{\mu}(\omega)$ and $d_{\lambda}(\omega)$ respectively [8]. The imaginary part of the damping functions corresponds to dissipation and the real part corresponds to dynamic stiffness. At 0 Hz the damping functions are equal to zero.

$$\hat{\mu} \stackrel{\text{def}}{=} \mu(1 + d_{\mu}), \quad \hat{\lambda} \stackrel{\text{def}}{=} \lambda(1 + d_{\lambda})$$

where

$$d_{\lambda}(\omega) \stackrel{\text{def}}{=} \sum_{l=1}^{N_a} \frac{\mathrm{i}\omega}{\mathrm{i}\omega + \beta_l} \cdot \frac{3\varphi_l^2 + 4\varphi_l \mu_l}{\lambda \cdot \alpha_l},$$

$$d_{\mu}(\omega) \stackrel{\text{def}}{=} \sum_{l=1}^{N_a} \frac{\mathrm{i}\omega}{\mathrm{i}\omega + \beta_l} \cdot \frac{2\mu_l^2}{\mu \cdot \alpha_l}.$$

α_l, β_l, μ_l, φ_l are AHL parameters and N_a is the number of assumed relaxation processes.

APPENDIX C: HIERARCHICAL POLYNOMIAL

The first eight hierarchical functions are

$$f_3(\chi) = \frac{1}{2}\chi^2 - \frac{1}{2}, \quad f_4(\chi) = \frac{1}{2}\chi^3 - \frac{1}{2}\chi, \quad f_5(\chi) = \frac{5}{8}\chi^4 - \frac{3}{4}\chi^2 + \frac{1}{8},$$

$$f_6(\chi) = \frac{7}{8}\chi^5 - \frac{5}{4}\chi^3 + \frac{3}{8}\chi, \quad f_7(\chi) = \frac{63}{48}\chi^6 - \frac{35}{16}\chi^4 + \frac{15}{16}\chi^2 - \frac{1}{16},$$

$$f_8(\chi) = \frac{99}{48}\chi^7 - \frac{63}{16}\chi^5 + \frac{35}{16}\chi^3 - \frac{5}{16}\chi,$$

$$f_9(\chi) = \frac{429}{128}\chi^8 - \frac{231}{32}\chi^6 + \frac{315}{64}\chi^4 - \frac{35}{32}\chi^2 + \frac{5}{128},$$

$$f_{10}(\chi) = \frac{715}{128}\chi^9 - \frac{429}{32}\chi^7 + \frac{693}{64}\chi^5 - \frac{105}{32}\chi^3 + \frac{35}{128}\chi.$$

APPENDIX D: DEFINITION OF FORMS $B(\cdot,\cdot)$ AND $F(\cdot)$

$$\begin{aligned} B(\mathbf{u}, \mathbf{v}) \stackrel{\text{def}}{=} & \hat{\mu}(u^s_{i,j}, v^s_{i,j})_\Omega + \hat{\mu}(u^s_{j,i}, v^s_{i,j})_\Omega + \hat{\lambda}(u^s_{j,j}, v^s_{i,i})_\Omega \\ & - \omega^2 \rho_{11}(u^s_i, v^s_i)_\Omega + \mathrm{i}\omega b(u^s_i, v^s_i)_\Omega, \\ & + Q(u^f_{j,j}, v^s_{i,i})_\Omega - \omega^2 \rho_{12}(u^f_i, v^s_i)_\Omega - \mathrm{i}\omega b(u^f_i, v^s_i)_\Omega, \\ & + Q(u^s_{j,j}, v^f_{i,i})_\Omega - \omega^2 \rho_{12}(u^s_i, v^f_i)_\Omega - \mathrm{i}\omega b(u^s_i, v^f_i)_\Omega, \\ & + R(u^f_{j,j}, v^f_{i,i})_\Omega - \omega^2 \rho_{22}(u^f_i, v^f_i)_\Omega + \mathrm{i}\omega b(u^f_i, v^f_i)_\Omega, \end{aligned} \tag{D.1a}$$

$$F(\mathbf{v}) \stackrel{\text{def}}{=} (\hat{T}_i, v^s_i)_{\Gamma_s} + \frac{Q}{R}(-p^f n_i, v^s_i)_{\Gamma_s} + \frac{Q}{3\hat{K}}(-p^s n_i, v^f_i)_{\Gamma_f} + (-p^f n_i, v^f_i)_{\Gamma_f}. \tag{D.1b}$$

APPENDIX E: BOUNDEDNESS OF $F(\cdot)$

Proposition 1. $\exists M,\ 0 < M < \infty : |F(\mathbf{v})| \leqslant M\|\mathbf{v}\|_{\mathscr{H}^1(\Omega)} \forall \mathbf{v} \in V \subset \mathscr{H}^1(\Omega)$
where

$$\|\mathbf{v}\|^2_{\mathscr{H}^1(\Omega)} \stackrel{\text{def}}{=} \sum_{i=1}^{3} (v_i, v_i)_\Omega + \sum_{i=1}^{3}\sum_{j=1}^{3} ((v^s_{i,j}, v^s_{i,j})_\Omega + (v^f_{i,j}, v^f_{i,j})_\Omega). \tag{E.1}$$

Proof. $F(\mathbf{v})$ may be written as $(\mathbf{A}, \mathbf{v})_\Gamma$, where $\mathbf{A}$ contains all prescribed boundary loads (which are finite). By the Cauchy–Schwartz inequality

$$|(\mathbf{A}, \mathbf{v})_\Gamma| \leqslant \|\mathbf{A}\|_{L^2(\Gamma)} \cdot \|\mathbf{v}\|_{L^2(\Gamma)}. \equiv C_1 \|\mathbf{v}\|_{L^2(\Gamma)}.$$

C_1 is finite since the boundary loads are finite. By the trace theorem [15]

$$\exists C_2 : \|\mathbf{v}\|_{L^2(\Gamma)} \leqslant C_2 \|\mathbf{v}\|_{\mathscr{H}^1(\Omega)}.$$

Let $M = C_1 C_2$ and hence

$$|F(\mathbf{v})| \leqslant M \|\mathbf{v}\|_{\mathscr{H}^1(\Omega)}.$$

APPENDIX F: MATERIAL DATA

Young's modulus	$E = 70{\cdot}0 \times 10^3$ Pa
The Poisson ratio	$v = 0{\cdot}39$
Porous material density	$\rho_m = 22{\cdot}1\,\mathrm{kg/m^3}$
Porosity	$\phi = 0{\cdot}98$
Fluid density	$\rho_0 = 1{\cdot}204\,\mathrm{kg/m^3}$
Fluid dynamic viscosity	$\mu^f = 1{\cdot}84 \times 10^{-5}$
Fluid ratio of specific heats	$\gamma = 1{\cdot}4$
Prandtl number	$Pr = 0{\cdot}71$
Viscous characteristic length	$\Lambda = 1{\cdot}1 \times 10^{-4}\,\mathrm{m}$
Thermal characteristic length	$\Lambda' = 7{\cdot}42 \times 10^{-4}\,\mathrm{m}$
Static flow resistivity of foam	$\sigma^{static} = 3{\cdot}75 \times 10^3\,\mathrm{kg/m^3 s}$
Tortuosity	$\alpha_\infty = 1{\cdot}17$
Thermal form factor	$M' = 0{\cdot}25$
Gas constant (for air)	$R^{gas} = 286{\cdot}7\,\mathrm{m^2/(s^2 K)}$
Absolute temperature	$T = 293{\cdot}15\,\mathrm{K}$

Augmented Hooke's law parameters

$$\alpha_1 = 1{\cdot}0, \quad \beta_1 = 3{\cdot}1416, \quad \varphi_1 = 71{\cdot}95, \; \mu_1 = 71{\cdot}30$$

$$\alpha_2 = 1{\cdot}0, \quad \beta_2 = 6{\cdot}28 \times 10^4, \quad \varphi_2 = 0, \; \mu_2 = 396{\cdot}74.$$

APPENDIX G: BIOT THEORY PARAMETERS

The parameters used in Biot's equations (1a) and (1b) b, ρ_{11}, ρ_{12}, ρ_{22}, Q, R are derived from the following relations [14] and the solid phase material parameters $\hat{\mu}$, $\hat{\lambda}$ are defined in Appendix B.

The kinematic viscosity

$$v^f = \mu^f / \rho_0. \tag{G.1}$$

The viscous permeability

$$k_0 = \mu^f / \sigma^{static}. \tag{G.2}$$

Frequency

$$\tilde{\omega} = \omega k_0 \alpha_\infty / v^f \phi. \tag{G.3}$$

Viscous-shaped factor

$$M = k_0 8\alpha_\infty / \phi \Lambda^2. \tag{G.4}$$

Viscous drag coefficient

$$b = \left(1 - \frac{M}{2}\,\mathrm{i}\tilde{\omega}\right)^{1/2} \sigma^{static} \phi^2. \tag{G.5}$$

Thermal static permeability

$$k_0' = M' \phi \Lambda'^2 / 8. \tag{G.6}$$

Inertial coupling factor

$$\rho_{12} = -\rho_0 \phi (\alpha_\infty - 1). \tag{G.7}$$

Corrected mass density for the solid phase

$$\rho_{11} = \rho_m - \rho_{12}. \tag{G.8}$$

Corrected mass density for the fluid phase

$$\rho_{22} = \rho_0 \phi - \rho_{12}. \tag{G.9}$$

Adiabatic bulk modulus for the fluid

$$K_a = \gamma R^{gas} T \rho_0. \tag{G.10}$$

Inverse thermal diffusivity

$$v' = v / Pr. \tag{G.11}$$

Thermal angular frequency

$$\tilde{\omega}' = \omega k_0' / v' \phi. \tag{G.12}$$

Thermal response factor

$$\beta = \gamma - (\gamma - 1)\left[1 - \frac{1}{\mathrm{i}\tilde{\omega}'}\left(1 - \frac{M'}{2}\,\mathrm{i}\tilde{\omega}'\right)^{1/2}\right]^{-1} \frac{1}{\phi}. \tag{G.13}$$

Corrected bulk modulus for the fluid

$$K_f = K_a / \beta. \tag{G.14}$$

Dilatational coupling factor

$$Q = (1 - \phi) K_f. \tag{G.15}$$

Homogenized bulk modulus of the fluid phase

$$R = K_f \phi. \tag{G.16}$$

APPENDIX H: NOMENCLATURE

OPERATORS AND FUNCTIONS

!	$n! = n\cdot(n-1)\cdot\cdots\cdot 1$ (faculty)
!!	$n!! = \begin{cases} n\cdot(n-2)\cdot\cdots\cdot 1 & n \text{ is odd} \\ n\cdot(n-2)\cdot\cdots\cdot 2 & n \text{ is even} \end{cases}$ (semi faculty)
int	integer part

Superscripts

$\hat{}$	the elastic parameter is augmented according to Appendix B
f	fluid part of porous medium
—	(overline) denotes complex conjugate
i	component ordinal number in Cartesian co-ordinate system
m, n, q, r	ordinal number of term in function series
s	solid part of porous medium
t	matrix transpose

Subscripts

FE	approximative solution using a finite element space
i, j, k	component ordinal number in Cartesian co-ordinate system
l	ordinal number of hierarchical polynomial
$,i$	partial derivative with respect to the Cartesian component x_i

Variables

b	viscous drag coefficient
$B(\cdot,\cdot)$	sesquilinear complex functional containing left-hand side in the weak formulation
$\mathbf{e}$	six-dimensional error function
$F(\cdot)$	antilinear complex functional containing loads and natural boundary conditions
K	bulk modulus of solid frame
n_i	unit normal vector outward the boundary
N	number of terms in function series
p	number of *hierarchical* polynomials
p^f	homogenized fluid phase pressure
p^s	homogenized pressure in the solid frame
Q	dilatational coupling factor between the fluid phase and the solid frame
R	bulk modulus of the fluid phase
u_i^s	displacement component in Cartesian co-ordinate direction i for the solid part m
u_i^f	displacement component in Cartesian co-ordinate direction i for the fluid part m
v_i^s	test function for displacement component in Cartesian co-ordinate direction i for the solid part
v_i^f	test function for displacement component in Cartesian co-ordinate direction i for the fluid part
$\mathbf{u}^s$	solid frame displacement vector
$\mathbf{u}^f$	fluid phase displacement vector
$\mathbf{v}^s$	solid frame displacement vector of test function
$\mathbf{v}^f$	fluid phase displacement vector of test functions
$\mathbf{u}$	six-dimensional displacement vector
$\mathbf{v}$	six-dimensional displacement vector of test functions

x_k	Cartesian co-ordinate component in direction k
$\mathbf{x}$	co-ordinate vector $\mathbf{x} = \{x_k\}$

Greek letters

μ	Lamé elastic parameter shear modulus
λ	Lamé elastic parameter
ρ_{11}	corrected mass density for the solid phase
ρ_{12}	inertial coupling factor
ρ_{22}	corrected mass density of the fluid phase ϕ porosity
σ_{ij}	Cauchy stress tensor
ω	angular velocity